RESEARCH ARTICLE | NOVEMBER 05 2024

A refined method for characterizing afterpulse probability in single-photon avalanche diodes

Special Collection: Advances in Quantum Metrology

B. Dejen 🗓 ; A. Vaquero-Stainer 🗓 ; T. S. Santana 🗓 ; L. Arabskyj 🗓 ; P. R. Dolan 🗓 ; C. J. Chunnilall 🗷 🗓



Appl. Phys. Lett. 125, 194002 (2024) https://doi.org/10.1063/5.0226118





Articles You May Be Interested In

Interference effects in commercially available free-space silicon single-photon avalanche diodes

Appl. Phys. Lett. (November 2024)

Low-noise photon counting above 100×10^6 counts per second with a high-efficiency reach-through single-photon avalanche diode system

Appl. Phys. Lett. (March 2021)

Custom single-photon avalanche diode with integrated front-end for parallel photon timing applications

Rev. Sci. Instrum. (March 2012)

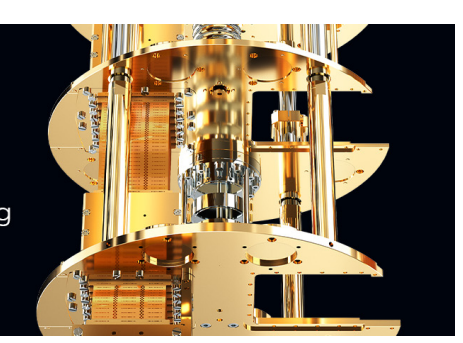


Accelerate your research.

Scale up your experiments with increased cooling power and a new side-loading LD system.

Discover the latest advances in cooling





A refined method for characterizing afterpulse probability in single-photon avalanche diodes

Cite as: Appl. Phys. Lett. 125, 194002 (2024); doi: 10.1063/5.0226118 Submitted: 29 June 2024 · Accepted: 25 October 2024 · Published Online: 5 November 2024

















AFFILIATIONS

¹National Physical Laboratory, Hampton Road, Teddington TW11 OLW, United Kingdom

 2 School of Physics, Engineering and Technology and York Centre for Quantum Technologies, University of York, York, YO10 5FT, United Kingdom

Note: This paper is part of the APL Special Collection on Advances in Quantum Metrology. ^{a)}Author to whom correspondence should be addressed: christopher.chunnilall@npl.co.uk

ABSTRACT

Single-photon avalanche diodes (SPADs) are critical components in low-light-level sensing and photonic quantum information applications. For these, it is often necessary that a full characterization of the SPAD is performed, for which a key metric is the afterpulse probability. This study provides a detailed comparison of the common synchronized and non-synchronized methods used to measure afterpulse probability. Measurements on a single SPAD reveal inconsistencies between the afterpulse probabilities obtained by the two methods. By re-deriving the equations from first principles, the discrepancy is traced to the analysis approach for the non-synchronized experiment. An improved analysis approach is presented, leading to better agreement between the non-synchronized and synchronized methods. The study also provides guidance on the experimental conditions required for the valid application of both methods, along with a detailed analysis of the limitations of the non-synchronized method under high photon flux. These findings offer a more accurate approach for characterizing afterpulse probability and for reconciling the results of two methods, which enables better quantification of SPAD performance.

© 2024 Author(s). All article content, except where otherwise noted, is licensed under a Creative Commons Attribution (CC BY) license (https:// creativecommons.org/licenses/by/4.0/). https://doi.org/10.1063/5.0226118

Single-photon avalanche diodes (SPADs) are non-photon-number-resolving "click"/"no-click" solid-state photodetectors capable of detecting light at the single-photon level, producing an output voltage pulse when a photon is detected. They are widely used in many research areas, 1-6 in part due to their relatively small physical footprint, broad spectral response, and low cost.

A non-ideal property of a SPAD is its afterpulsing behavior. An afterpulse is a spurious detection event originating from the release of charge carriers trapped in defect states during the preceding avalanche event.^{8,9} The release of a charge carrier is a probabilistic and timedependent process; hence, the afterpulse probability is defined as the probability that an afterpulse is generated in a given time window succeeding an event; 10 the total afterpulse probability is a timeindependent quantity defined as the total probability that an afterpulse is generated succeeding an event.

A number of methods have been proposed to suppress the afterpulse probability. These can be grouped into techniques which modify a SPAD's intrinsic properties such as temperature, hold-off time, excess bias, and capacitance; and photoionisation of trapped carriers, and post-processing techniques such as signal comparison, 13 and selfdifferencing. 14,15 While these methods have been shown to reduce afterpulsing probability, there are inherent tradeoffs and an implementation that completely eliminates afterpulses is yet to be demonstrated.

For many applications, accurate characterization of afterpulse probability is required. An example is quantum key distribution 1,16 where afterpulses not only increase the quantum bit error rate, lowering the secret key rate, but are also correlated with previous events, potentially causing information leakage. Knowledge of the afterpulse probability allows for optimization of detector parameters and hence the key rate. Methods used to characterize afterpulse probability can be loosely categorized into those which model the mechanisms responsible for afterpulses, and those which do not. The former includes single or multiple discrete, 17-19 and continuous 20-22 models of the energy distribution of defect states. Notably, it was shown in Ref. 23 that the afterpulse probability for different SPADs is best approximated by fundamentally different mathematical models, even when the SPADs are nominally identical, so in practice they must be individually characterized using methods that do not require models. Examples of these

10

 10^2

 10^{0}

methods include $g^{(2)}(\tau)$ measurements, 13,24 auto-correlation methods, $^{25-28}$ and methods based on time-correlated single-photon counting (TCSPC). $^{23,29-31}$

In this paper, we refer to the auto-correlation (time-difference) method in Sec. 15.5 of Ref. 28, which is similar to that used in Refs. 25 and 26, as the non-synchronized method, and to the method based on pulsed excitation and TCSPC used in Refs. 23 and 31 and Method 4 in Sec. 15.6 of Ref. 28 as the synchronized method. The synchronized method is advantageous because the different click sources can be easily distinguished, which makes the total afterpulse probability calculation straightforward. However, this method cannot be used to reliably determine the time dependence of the afterpulse probability and requires an appropriate pulsed source with suitable duration, extinction ratio, and repetition rate which might not be readily available. In contrast, the non-synchronized method is less resource-intensive, i.e., can be performed using only the intrinsic dark counts of the SPAD, or with a CW laser, and is suitable for measuring both the time dependence of the afterpulse probability and the total afterpulse probability. However, more steps are necessary to distinguish the contributions of different click sources, and as we show in this paper, the method is only valid under certain experimental conditions.

Consistency between these methods has not been proven. Here, we report a direct comparison of the synchronized and non-synchronized methods performed on the same SPAD. We show that an inconsistency between the afterpulse probabilities measured by the synchronized and non-synchronized methods arises as a consequence of the analysis for the non-synchronized method. We propose an alternative and show that this provides better agreement across a wide range of detector dead-times. We then use this method to measure the dependence of the afterpulse probability on photon flux and highlight the limitations on the experimental conditions under which the afterpulse probability can be reliably characterized.

In the synchronized method, a pulse generator (Tektronix AWG70001) was used to send synchronized signals to the start channel of the time-tagging module (FAST ComTec GmbH MCS6A operated in multi-stop mode) and to trigger emission from a 1550 nm pulsed laser (PicoQuant LDH-P-F-N-1550), which was attenuated to the desired power by a variable optical attenuator (VOA, Hewlett Packard 8158B) before coupling into an ID Quantique ID230 SPAD—see Fig. 1(a). The time-differences between the SPAD clicks and the immediately preceding start signal were recorded on a computer, and a histogram with 1 μ s bin-widths was generated as shown in Fig. 1(b).

Detections from the pulsed laser occur in the first time bin (green dotted line) in Fig. 1(b), and the afterpulses originating from these clicks cause a second decaying feature after the dead time of $10~\mu s$. A small number of clicks are measured between these that occur in clock cycles when there are no detections from the pulsed laser. Dark counts and their afterpulses are uncorrelated with the clock signal from the pulse generator and hence form a uniform background in the histogram. The background value is the mean value of the histogram in the bins after the afterpulses have decayed. The background-subtracted histogram contains only pulsed laser detections and their afterpulses. The ratio of the two is equal to the number of afterpulses generated per detection event, $n_{\rm ap}$, and is expressed as

$$n_{\rm ap} = \frac{\sum_{N \in \Gamma_{\rm ap}} \operatorname{Clicks}(N)}{\sum_{N \in \Gamma_{\rm laser}} \operatorname{Clicks}(N)},\tag{1}$$

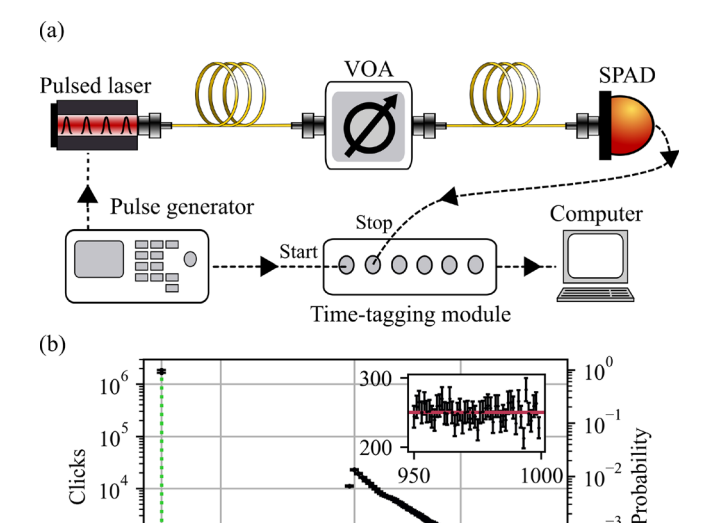


FIG. 1. (a) Experimental setup for the synchronized method. (b) Clicks histogram and probability distribution (black) measured using a pulsed laser with a 1 kHz repetition rate incident on the ID Quantique ID230, set to 10 μ s dead time, 20% detection efficiency, and a temperature of 183.15 K. The uniform background level is indicated by a solid red line. The inset shows the region of the histogram used to calculate the uniform background level.

10¹

Time after laser pulse / μs

 10^2

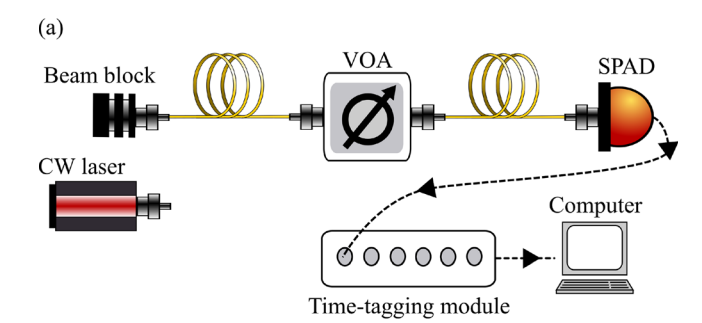
10

where N is the set of bin-numbers equal in length to the histogram and Γ_{laser} and Γ_{ap} are the set of bin numbers containing the laser pulses and their afterpulses, respectively. In Fig. 1(b), Γ_{laser} and Γ_{ap} correspond to the bin highlighted by the dashed-green line and bins after $\approx 10 \mu s$, respectively. Since the probability of each afterpulse-order is taken to follow a geometric distribution, 31 the infinite sum of a geometric distribution is used to correct for the presence of higher order afterpulses (see the supplementary material). In doing so, the total afterpulse probability is calculated by

$$P_{\text{ap total}}^{(A)} = \frac{n_{\text{ap}}}{1 + n_{\text{ap}}}.$$
 (2)

For accurate implementation of this method, the repetition rate of the laser must be such that the entirety of the afterpulse distribution occurs between laser pulses so that the background level can be determined, and its pulse width must be significantly shorter than the dead time of the SPAD to distinguish between the photon detection and afterpulse clicks.

In the non-synchronized method, analysis is performed on dark counts. Low flux CW light can be used to increase the click rate, while maintaining the average time difference between clicks to be much longer than the dead time of the SPAD. This should be implemented with care as the total afterpulse probability measured is flux dependent, as shown later. Throughout, we assume that the SPAD recovers the same state, on average, after a detection event.²⁶ In the setup illustrated in Fig. 2(a), the clicks were time-stamped on a single channel of the



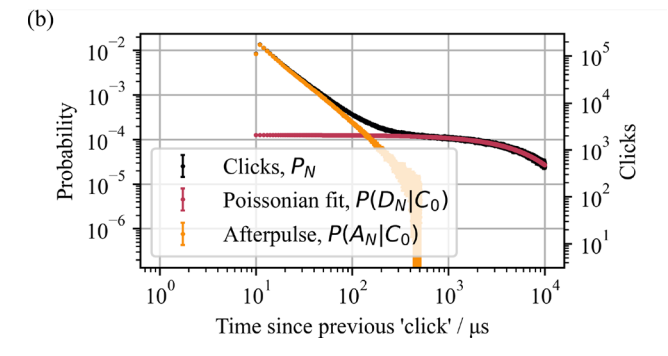


FIG. 2. (a) Experimental setup for the non-synchronized method. The laser can be substituted for the beam block (no light source) to perform the measurements with CW light. (b) Clicks histogram and probability distributions measured by the non-synchronized method using only dark counts on the ID Quantique ID230, set to $10~\mu s$ dead time, 20% detection efficiency, and a temperature of 183.15 K. The histogram bins are $1~\mu s$ wide.

time-tagging module and recorded on a computer. The time differences between consecutive clicks were used to calculate the probability that a click was measured in a given time bin after a previous click, P_N . This is referred to as the click interval probability distribution, and an example of this is shown in Fig. 2(b).

The click interval probability distribution is expressed as

$$P_N = P(C_N, \overline{C}_{N-1}, ..., \overline{C}_1 | C_0), \tag{3}$$

where C_i ($\overline{C_i}$) indicate whether there was (not) a click in the ith time bin. This reads as the probability that a click was measured in the Nth time bin and no clicks were measured between the first and (N-1)th time bins inclusive, given that a click occurred in the zeroth time bin. This exactly describes the probability distribution generated for the time difference between consecutive clicks, wherein the first click is said to have occurred in the zeroth time bin, and the second click occurs in the Nth time bin. Two equivalent ways in which Eq. (3) can be factorized are

$$P_N = P(\overline{C}_{N-1}, \dots, \overline{C}_1 | C_N, C_0) P(C_N | C_0), \tag{4}$$

and

$$P_N = P(C_N | \overline{C}_{N-1}, ..., \overline{C}_1, C_0) P(\overline{C}_{N-1}, ..., \overline{C}_1 | C_0).$$
 (5)

Equation (4) is expressed in a particularly useful way. Since, by definition, if a click occurred in the Nth time bin following a previous click, then no clicks occurred in the N-1 preceding time bins, hence $P(\overline{C}_{N-1},...,\overline{C}_1|C_N,C_0)=1$. Therefore, it follows that

$$P_N = P(C_N|C_0), (6)$$

$$=1-P(\overline{D}_N|C_0)P(\overline{A}_N|C_0), \qquad (7)$$

$$= 1 - [1 - P(D_N|C_0)][1 - P(A_N|C_0)], \tag{8}$$

where we have distinguished the Poissonian clicks, i.e., dark counts and CW light, denoted D, and afterpulse clicks, denoted A. $P(A_N|C_0)$ and $P(D_N|C_0)$ are the probabilities that the subsequent click occurs in the Nth time bin and is an afterpulse or Poissonian click, respectively. Written in this way, it is clear that $P(A_N|C_0)$ is the time dependence of the afterpulse probability. The total afterpulse probability can then be expressed as

$$P_{\text{ap total}}^{(B)} = \sum_{N=1}^{\infty} P(A_N | C_0). \tag{9}$$

To determine $P(A_N|C_0)$, $P(D_N|C_0)$, must be calculated first. The afterpulse probability typically decays much faster than the Poissonian probability distribution 23 and we define the afterpulse lifespan $\tau_{\rm ap} = N_{\rm ap} \Delta T$ as the time after which the afterpulse probability distribution has become negligible, i.e., $P(A_{N>N_{\rm ap}}|C_0) \ll P(D_{N>N_{\rm ap}}|C_0)$. The clicks occurring in time bins $N>N_{\rm ap}$ are attributed only to Poissonian sources and hence follow the distribution

$$P(D_N|C_0) = a[\exp(r_m \Delta T) - 1]\exp(-r_m N \Delta T), \tag{10}$$

where a is the amplitude and r_m is equivalent to a rate, but is notably not equal to the Poissonian detection rate. Notes on the physical meaning of a and r_m can be found in the supplementary material. This fit, illustrated by the red curve in Fig. 2(b), was extrapolated to time bins $N \leq N_{\rm ap}$ after which Eq. (8) was used to calculate $P(A_N|C_0)$.

It could be misconstrued that the afterpulse probability distribution measured by the non-synchronized method is equivalent to the one measured by the synchronized method, which is derived by dividing the background-subtracted histogram by the number of pulsed laser detection events. Figure 3 shows that the distributions agree only for a duration equivalent to one dead time after the detector is active, where the main source of clicks is first-order afterpulses. Beyond this, the distribution generated by the non-synchronized method diverges from the synchronized distribution due to higher order afterpulses, i.e.,

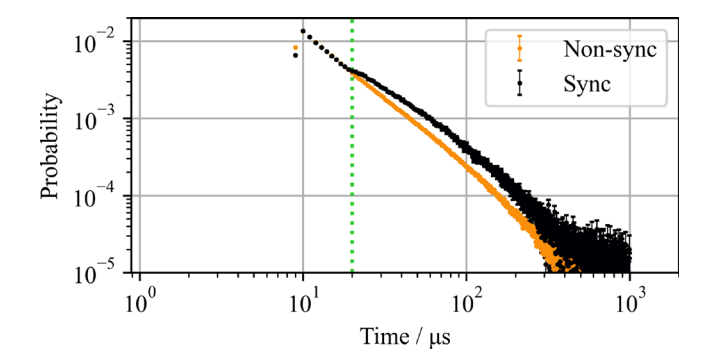
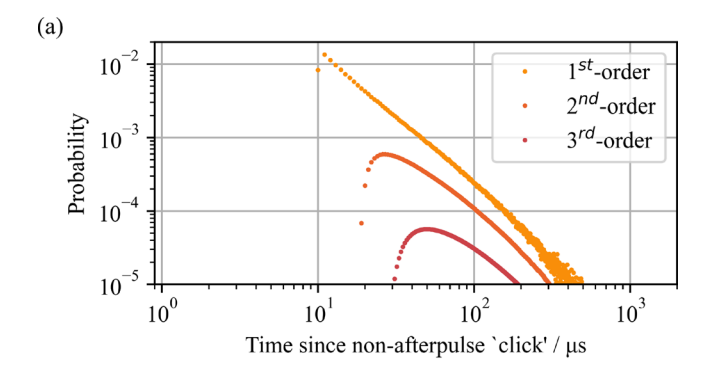


FIG. 3. Afterpulse probability distributions measured by the non-synchronized and synchronized methods on the ID Quantique ID230, set to 10 μ s dead time, 20% detection efficiency, and a temperature of 183.15 K. The bin corresponding to one dead time after the detector is active is indicated by the green dotted line. The histogram bins are 1 μ s wide.



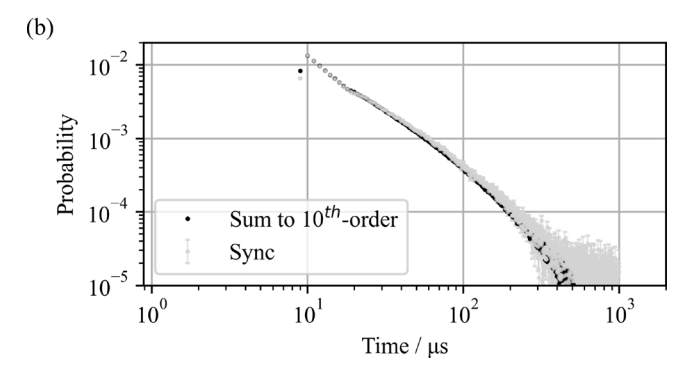


FIG. 4. (a) The first-order afterpulse probability distribution measured by the non-synchronized method using only dark counts, and the second- and third-order afterpulse probability distributions. (b) Afterpulse probability distribution measured by the synchronized method and the sum of afterpulse probability distributions measured by the non-synchronized method up to the tenth-order.

afterpulses originating from afterpulses. A method for reconstructing the probability distribution measured by the synchronized experiment from the distribution measured by the non-synchronized experiment, by considering higher order afterpulses, is presented in the supplementary material. Figure 4(a) shows the results from this analysis, and the close similarity of the probability distributions in Fig. 4(b) shows that the method can be used to reconcile the synchronized and non-synchronized methods.

As previously noted, Eq. (3) can be factored in two useful ways. Further factorization of Eq. (5) leads to

$$P_{N} = \left[1 - P(\overline{D}_{N}|\overline{C}_{N-1}, ..., \overline{C}_{1}, C_{0})P(\overline{A}_{N}|\overline{C}_{N-1}, ..., \overline{C}_{1}, C_{0})\right] \times \prod_{n=1}^{N-1} \left[P(\overline{D}_{n}|\overline{C}_{n-1}, ..., \overline{C}_{1}, C_{0})P(\overline{A}_{n}|\overline{C}_{n-1}, ..., \overline{C}_{1}, C_{0})\right].$$

$$(11)$$

Using Bayes' theorem and the property of Poissonian clicks—that they have a fixed probability of occurring in any time bin if the time bins are of the same duration—Eq. (11) can be simplified to

$$P_{N} = \left[1 - P(\overline{D})P(\overline{A}_{N}|\overline{C}_{N-1},...,\overline{C}_{1},C_{0})\right] \times P(\overline{D})^{N-1} \prod_{n=1}^{N-1} P(\overline{A}_{n}|\overline{C}_{n-1},...,\overline{C}_{1},C_{0}),$$
(12)

which is equivalent to Eq. (5) in Ref. 26 and Eq. (15.4b) in Ref. 28. The derivation of Eq. (12) can be found in the supplementary material.

In this paper, we make explicit comparisons with the method outlined in Sec. 15.5 of Ref. 28, in which the term equivalent to $P(A_N|\overline{C}_{N-1},...,\overline{C}_1,C_0)$ is defined as the first-order afterpulse probability in the Nth time bin. This term reads as the probability of measuring an afterpulse click in the Nth time bin given that there was a click in the zeroth time bin and no clicks in the intermediate time bins. Note that this is not equal to $P(A_N|C_0)$, and the difference is elaborated on later. For the purposes of comparison, we use only the total afterpulse probability up to first-order, which is defined in Ref. 28 as equivalent to

$$P_{\text{ap total}}^{(C)} = \sum_{n=1}^{\infty} P(A_n | \overline{C}_{n-1}, ..., \overline{C}_1, C_0).$$
 (13)

It should be noted that the inclusion of higher order terms as defined in Ref. 28 would increase $P_{\text{an total}}^{(C)}$.

For the ID Quantique ID230 SPAD, one can adjust the dead time between 2 and $100~\mu s$, detection probability between 0% and 25%, and the temperature between 183.15 and 223.15 K. Figure 5 shows the total afterpulse probability measured at different detector dead time settings with the detection probability and temperature set at 20% and 183.15 K, respectively. The measurements applying the non-synchronized method were performed without illumination of the SPAD, and in the synchronized method, the laser generated pulses with FWHM < 40 ps at a repetition rate of 1 kHz. These results demonstrate that the agreement between the synchronized method and the non-synchronized method when analyzed with Eqs. (2) and (9) are significantly better than when Eq. (12) is used in the non-synchronized method.

A closer examination of the mathematical relationship between $P_{ap\, total}^{(B)}$ and $P_{ap\, total}^{(C)}$ predicts the measured divergence. It can be shown that the afterpulse probability distributions defined in Eqs. (9) and (13) are related by

$$P(\overline{C}_{N-1}, ..., \overline{C}_1 | C_0) = \frac{P(A_N | C_0)}{P(A_N | \overline{C}_{N-1}, ..., \overline{C}_1, C_0)}.$$
 (14)

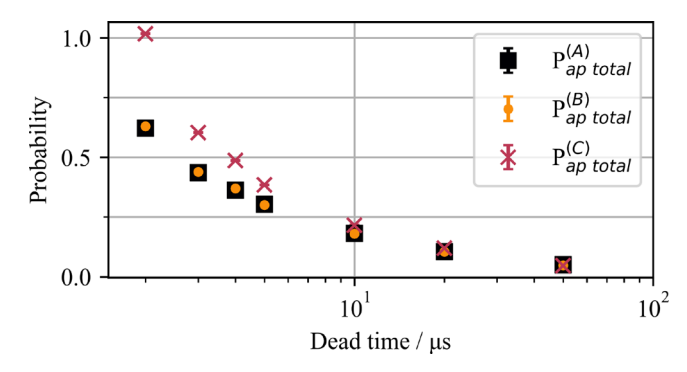


FIG. 5. Total afterpulse probability measured at different dead time settings for the ID Quantique ID230 by the synchronized method (A), and the non-synchronized method with our proposed analysis method (B), and the previous analysis method (C)

 $P(\overline{C}_{N-1},...,\overline{C}_1|C_0)$ is the probability of not measuring a click in time bins 1 to N-1 given that there was a click in the zeroth time bin. As the dead time is decreased, the number of trapped charge carriers that can cause an afterpulse increases. This increases the probability that clicks occur with shorter time differences, which corresponds to a decrease in $P(\overline{C}_{N-1},...,\overline{C}_1|C_0)$. Since $P(\overline{C}_{N-1},...,\overline{C}_1|C_0) \leq 1$, $P(A_N|C_0) \leq P(A_N|\overline{C}_{N-1},...,\overline{C}_1,C_0)$ for N>1 and therefore $P_{\text{ap total}}^{(B)}$ and $P_{\text{ap total}}^{(C)}$ diverge. The derivation of Eq. (14) can be found in the supplementary material.

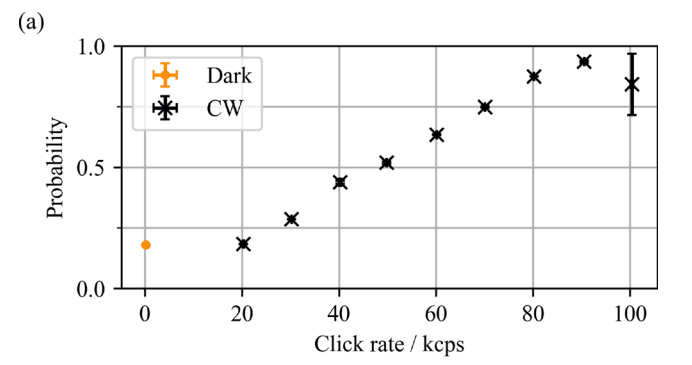
The difference between $P_{ap\,total}^{(B)}$ and $P_{ap\,total}^{(C)}$ can also be understood by considering the conditions for $P(A_N|C_0)$ and $P(A_N|\overline{C}_{N-1},...,\overline{C}_1,C_0)$. In the former, the condition is that there was a click in the zeroth time bin, which is satisfied by all of the events in the time-difference histogram. In the latter, the condition is that there was a click in the zeroth time bin and no clicks in time bins 1 to N-1, which is satisfied by only a subset of events in the time-difference histogram. Therefore, the number of events in which an afterpulse click occurs in the Nth time bin constitutes a smaller proportion of the former than the latter, hence $P(A_N|C_0) \leq P(A_N|\overline{C}_{N-1},...,\overline{C}_1,C_0)$ for N>1.

For some applications, an accurate quantification of the afterpulse probability dependence on photon flux is critical, such as for the characterization of SPAD detection efficiency. To investigate this, we used a laser diode (Thorlabs LP1550-SAD2) shown in Fig. 2(a) and measured the total afterpulse probability using the non-synchronized method over a range of SPAD click rates. The results are presented in Fig. 6(a) alongside the total afterpulse probability measured without illumination of the SPAD. The total afterpulse probabilities measured at the dark count level and at 20 kcps are similar (<2% difference), but increase rapidly for click rates greater than this, up to almost unity near saturation. The increase arouses suspicion because the predominant cause of afterpulses, release of charge from defect states, ¹⁷ should not be strongly dependent on photon-flux.

Two potential explanations have been identified. First, the non-synchronized method requires the Poissonian distribution to be determined from fitting of Eq. (10) to P_N . Figure 6(b) shows the coefficient of determination, R^2 , measured on the fit at each click rate, decreases as the click rate increases, implying that it becomes increasingly difficult to distinguish a Poissonian probability distribution within the click interval probability distribution. This is intuitive since a decrease in the mean time between Poissonian events leads to a faster decay of the click interval probability distribution and therefore greater overlap of Poissonian and afterpulse events in the histogram, making the distinction harder. Second, there is the possibility that for the dead time selected, a non-negligible fraction of the charge remains trapped at defect sites after an event, causing an overall increase in the number of trapped states as the increasing laser power reduces the mean time between photon emissions.

These results highlight potential limitations of using the nonsynchronized method for measuring the total afterpulse probability with added photon fluxes; further work is planned to assess whether the total afterpulse probability can be accurately measured under these conditions.

In conclusion, we have demonstrated that the synchronized and non-synchronized methods described in the literature give diverging estimates of the afterpulse probability, especially at shorter detector



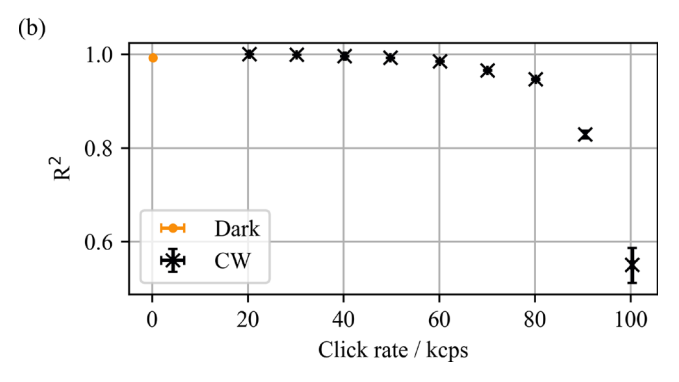


FIG. 6. (a) Total afterpulse probability measured on experimental data by the non-synchronized method and (b) R^2 measured for the Poissonian probability distribution fit. The values measured when the SPAD was not illuminated are shown in orange. The results are for the ID Quantique ID230, set to 10 μ s dead time, 20% detection efficiency, and a temperature of 183.15 K.

dead-times. We proposed an alternative analysis method for the non-synchronized method and demonstrated that it generated better agreement with the results of the synchronized method, for measurements on an ID Quantique ID230 SPAD. We also presented experimental results, which highlight limitations of this method for measuring the afterpulse probability with added photon-flux. The methodologies presented in this paper can be used to inform full in-depth characterizations of SPAD modules and a future revision of the ETSI standard GS QKD 011. ²⁸

See the supplementary material for additional notes and derivations of various equations.

This work was supported by the U.K. government department for Science, Innovation and Technology through the U.K. national quantum technologies programme. B.D., T.S.S., L.A., P.R.D., and C.J.C. also acknowledge funding from the Innovate UK Industrial Strategy Challenge Fund Project No. 106374-49229 "Assurance of Quantum Random Number Generators (AQuRand)" and Project No. 19NRM06 METISQ which received funding from the EMPIR programme co-financed by the Participating States and from the European Union's Horizon 2020 research and innovation programme. A.V.-S. is supported by the UK EPSRC Quantum Communications Hub, Grant No. EP/T001011/1.

AUTHOR DECLARATIONS Conflict of Interest

The authors have no conflicts to disclose.

Author Contributions

B. Dejen: Conceptualization (equal); Formal analysis (lead); Investigation (supporting); Methodology (equal); Software (lead); Validation (equal); Visualization (lead); Writing – original draft (equal); Writing – review & editing (equal). A. Vaquero-Stainer: Conceptualization (equal); Formal analysis (supporting); Investigation (lead); Methodology (equal); Software (supporting); Validation (equal); Visualization (supporting); Writing – original draft (equal); Writing – review & editing (equal). T. S. Santana: Methodology (equal); Validation (equal); Writing – review & editing (supporting). L. Arabskyj: Conceptualization (supporting); Investigation (supporting); Validation (supporting); Writing – review & editing (supporting). P. R. Dolan: Conceptualization (equal); Formal analysis (supporting); Funding acquisition (supporting); Supervision (equal); Visualization (supporting); Writing – review & editing (equal). C. J. Chunnilall: Funding acquisition (lead); Supervision (equal); Visualization (supporting); Writing – review & editing (lead).

DATA AVAILABILITY

The data that support the findings of this study are available from the corresponding author upon reasonable request.

REFERENCES

- ¹F. Ceccarelli, G. Acconcia, A. Gulinatti, M. Ghioni, I. Rech, and R. Osellame, "Recent advances and future perspectives of single-photon avalanche diodes for quantum photonics applications," Adv. Quantum Technol. 4, 2000102 (2021).
- ²W. Whitehead, Z. Nelson, K. Y. Camsari, and L. Theogarajan, "CMOS-compatible Ising and Potts annealing using single-photon avalanche diodes," Nat. Electron. 6, 1009–1019 (2023).
- ³G. Acconcia, F. Ceccarelli, A. Gulinatti, and I. Rech, "Timing measurements with silicon single photon avalanche diodes: Principles and perspectives," Opt. Express 31, 33963–33999 (2023).
- ⁴A. F. Bulling and I. Underwood, "Pion detection using single photon avalanche diodes," Sensors 23, 8759 (2023).
- ⁵H. Chen, X. Chen, J. Lu, X. Liu, J. Shi, L. Zheng, R. Liu, X. Zhou, and P. Tian, "Toward long-distance underwater wireless optical communication based on a high-sensitivity single photon avalanche diode," IEEE Photonics J. 12, 1–10 (2020).
- ⁶K. Kuzmenko, P. Vines, A. Halimi, R. J. Collins, A. Maccarone, A. McCarthy, Z. M. Greener, J. Kirdoda, D. C. Dumas, L. F. Llin *et al.*, "3D LIDAR imaging using Ge-on-Si single-photon avalanche diode detectors," Opt. Express 28, 1330–1344 (2020).
- ⁷M. D. Eisaman, J. Fan, A. Migdall, and S. V. Polyakov, "Invited review article: Single-photon sources and detectors," Rev. Sci. Instrum. 82, 071101 (2011).
- ⁸C. J. Chunnilall, I. P. Degiovanni, S. Kück, I. Müller, and A. G. Sinclair, "Metrology of single-photon sources and detectors: A review," Opt. Eng. 53, 081910 (2014).
- ⁹S. Cova, M. Ghioni, A. Lacaita, C. Samori, and F. Zappa, "Avalanche photodiodes and quenching circuits for single-photon detection," Appl. Opt. 35, 1956–1976 (1996).
- ¹⁰J. C. Bienfang, T. Gerrits, P. S. Kuo, A. Migdall, S. Polyakov, and O. Slattery, "Single-photon sources and detectors dictionary," NIST IR 8486 (National Institute of Standards and Technology, Gaithersburg, MD, 2023).
- ¹¹J. Zhang, M. A. Itzler, H. Zbinden, and J.-W. Pan, "Advances in InGaAs/InP single-photon detector systems for quantum communication," Light Sci. Appl. 4, e286–e286 (2015).
- ¹²S.-B. Cho and S.-K. Kang, "Weak avalanche discrimination for gated-mode single-photon avalanche photodiodes," Opt. Express 19, 18510–18515 (2011).

- ¹³M. A. Krainak, "Photoionization of trapped carriers in avalanche photodiodes to reduce afterpulsing during Geiger-mode photon counting," in *Conference on Lasers and Electro-Optics (CLEO)* (IEEE, 2005), Vol. 1, pp. 588–590.
- ¹⁴C. Healey, I. Lucio-Martinez, M. R. Lamont, X. Mo, and W. Tittel, "Characterization of an InGaAs/InP single-photon detector at 200 MHz gate rate," arXiv:1105.3760 (2011).
- ¹⁵Z. L. Yuan, B. E. Kardynal, A. W. Sharpe, and A. J. Shields, "High speed single photon detection in the near infrared," Appl. Phys. Lett. 91, 041114 (2007).
- ¹⁶J. Liu, Y. Xu, Z. Wang, Y. Li, Y. Gu, Z. Liu, and X. Zhao, "Reducing afterpulsing in InGaAs (P) single-photon detectors with hybrid quenching," Sensors 20, 4384 (2020).
- 17 S. Cova, A. Lacaita, and G. Ripamonti, "Trapping phenomena in avalanche photodiodes on nanosecond scale," IEEE Electron Device Lett. 12, 685–687 (1991).
- ¹⁸C. Wiechers, R. Ramírez-Alarcón, O. R. Muñiz-Sánchez, P. D. Yépiz, A. Arredondo-Santos, J. G. Hirsch, and A. B. U'Ren, "Systematic afterpulsing-estimation algorithms for gated avalanche photodiodes," Appl. Opt. 55, 7252–7264 (2016).
- ¹⁹B. Korzh, T. Lunghi, K. Kuzmenko, G. Boso, and H. Zbinden, "Afterpulsing studies of low-noise InGaAs/InP single-photon negative-feedback avalanche diodes," J. Mod. Opt. 62, 1151–1157 (2015).
- ²⁰M. A. Itzler, M. Entwistle, and X. Jiang, "High-rate photon counting with Geiger-mode APDs," in *IEEE Photonic Society 24th Annual Meeting* (IEEE, 2011), pp. 348–349.
- ²¹M. A. Itzler, X. Jiang, and M. Entwistle, "Power law temporal dependence of InGaAs/InP SPAD afterpulsing," J. Mod. Opt. 59, 1472–1480 (2012).
- ²²D. Horoshko, V. Chizhevsky, and S. Y. Kilin, "Afterpulsing model based on the quasi-continuous distribution of deep levels in single-photon avalanche diodes," J. Mod. Opt. 64, 191–195 (2017).
- ²³A. W. Ziarkash, S. K. Joshi, M. Stipčević, and R. Ursin, "Comparative study of afterpulsing behavior and models in single photon counting avalanche photo diode detectors," Sci. Rep. 8, 5076 (2018).
- ²⁴Y.-S. Kim, Y.-C. Jeong, S. Sauge, V. Makarov, and Y.-H. Kim, "Ultra-low noise single-photon detector based on Si avalanche photodiode," Rev. Sci. Instrum. 82, 093110 (2011).
- ²⁵A. Yoshizawa, R. Kaji, and H. Tsuchida, "Quantum efficiency evaluation method for gated-mode single-photon detector," Electron. Lett. 38, 1468–1469 (2002).
- ²⁶G. Humer, M. Peev, C. Schaeff, S. Ramelow, M. Stipčević, and R. Ursin, "A simple and robust method for estimating afterpulsing in single photon detectors," J. Lightwave Technol. 33, 3098–3107 (2015).
- ²⁷M. A. Wayne, J. C. Bienfang, and S. V. Polyakov, "Simple autocorrelation method for thoroughly characterizing single-photon detectors," Opt. Express 25, 20352–20362 (2017).
- ²⁸See https://www.etsi.org/deliver/etsi_gs/qkd/001_099/011/01.01.01_60/gs_qkd 011v010101p.pdf for "Quantum Key Distribution (QKD); Component characterization: Characterizing optical components for QKD systems," ETSI GS QKD 011 V1.1.1 (2016).
- 29J. Zhang, R. Thew, J.-D. Gautier, N. Gisin, and H. Zbinden, "Comprehensive characterization of InGaAs-InP avalanche photodiodes at 1550 nm with an active quenching ASIC," IEEE J. Quantum Electron. 45, 792–799 (2009).
- ³⁰J. Oh, C. Antonelli, M. Tur, and M. Brodsky, "Method for characterizing single photon detectors in saturation regime by cw laser," Opt. Express 18, 5906–5911 (2010)
- ³¹G. Kawata, J. Yoshida, K. Sasaki, and R. Hasegawa, "Probability distribution of after pulsing in passive-quenched single-photon avalanche diodes," IEEE Trans. Nucl. Sci. 64, 2386–2394 (2017).
- ³²D. Bronzi, F. Villa, S. Tisa, A. Tosi, and F. Zappa, "SPAD figures of merit for photon-counting, photon-timing, and imaging applications: A review," IEEE Sens. J. 16, 3–12 (2016).
- ³³T. Gerrits, A. Migdall, J. C. Bienfang, J. Lehman, S. W. Nam, J. Splett, I. Vayshenker, and J. Wang, "Calibration of free-space and fiber-coupled single-photon detectors," Metrologia 57, 015002 (2020).
- 34⁴ M. López, H. Hofer, and S. Kück, "Detection efficiency calibration of single-photon silicon avalanche photodiodes traceable using double attenuator technique," J. Mod. Opt. 62, 1732–1738 (2015).
- ³⁵C. J. Chunnilall, G. Lepert, J. J. Allerton, C. J. Hart, and A. G. Sinclair, "Traceable metrology for characterizing quantum optical communication devices," Metrologia 51, S258-S286 (2014).